CHAPTER 6

SOLVENT EFFECTS ON RADIATIVE AND NON-RADIATIVE EXCITED STATE DECAYS

AURORA MUÑOZ LOSA, IGNACIO FDEZ. GALVÁN, M. ELENA MARTÍN, AND MANUEL A. AGUILAR

Química Física, Universidad de Extremadura, Avda. de Elvas s/n. 06071 Badajoz (Spain)

Abstract: An extended version of the ASEP/MD method that permits the unified treatment of solvent effects on both radiative and non-radiative excited state decays is presented. The method combines a high-level quantum-mechanic description of the ground and excited states of the solute molecule with molecular dynamics simulations of the solvent. De-excitations are intrinsically dynamic processes where there exists an interplay between electronic structure and nuclear dynamics. We have undertaken this problem by establishing two limit situations, which we have characterized as equilibrium and non-equilibrium solvation regimes. In the former, we suppose decay times long enough to allow a complete relaxation of the solute and the solvent structure. In the latter, we suppose the decay process is fast enough to prevent the solvent equilibration. As an example of application of the methodology the solvent effects on radiative and non-radiative de-excitation processes in acrolein are studied

6.1. INTRODUCTION

The study of solvent effects on the appearance of UV-vis absorption spectra has a long history [1]. From the first qualitative (classical) description based on the changes in the dipole moment and polarizability during the excitation until the current quantitative models where the solute charge distribution is described through high-level quantum-mechanics techniques, a great number of theoretical models have been proposed [2,3,4,5] in such a way that, at present, the chemists have at their disposition a wide range of methods that permit the prediction of the position and intensity of the absorption bands of chromophores in solution. Comparatively, less attention has been paid to the study of solvent effects on emission spectra (fluorescence and phosphorescence) [6,7] where only recently we have begun to have available accurate methods that permit to optimize the geometry and charge distribution of excited states and to describe its interaction with the solvent. Solvent effects on emission spectra follow qualitative rules similar to those applied to absorption spectra [8,9]: a band in the fluorescence or phosphorescence spectrum will

S. Canuto (ed.), Solvation Effects on Molecules and Biomolecules, 135–157.
DOI 10.1007/978-1-4020-8270-2_6, © Springer Science+Business Media B.V. 2008

shift to higher frequencies (blue shift) if the dipole moment of the excited state is smaller than the ground state dipole moment and it will be red shifted if the dipole moment of the excited state is larger than the ground state dipole moment. In general, the magnitude of the solvent shift will increase with the solvent polarity and with the variation of the dipole moment during the transition. However, even when one has the dipole moment values for the solute molecule in the different states (something not always easy because they must be calculated at the excited state optimized geometry) these approximate rules could fail when applied to molecules with complex charge distributions or when specific solute–solvent interactions are involved.

Unlike UV-vis absorption spectra where all molecules display one or more active bands, many molecules do not present emission spectra or if they do, they exhibit exceedingly small quantum yield values. To understand this behaviour, one must realize that radiative decay always competes with non-radiative decay pathways, mainly internal conversion (IC), intersystem crossing (ISC) and quenching. Solvents can favour the activation of non-radiation pathways, consequently, they can have a dramatic influence on the fluorescence quantum yields. So, for instance, molecules can display fluorescence spectra in some solvent but not in another [10]. Despite the proved importance of the molecular environment, the theoretical study of solvent effects on IC and ISC (quenching is a phenomenon that depends on the presence in the solvent of certain type of molecules, oxygen for instance and not on the characteristics of the excited state) has received little attention [11,12,13,14,15,16,17,18]. The reasons are obvious: to the difficulties inherent to the study of non-adiabatic processes (processes that imply more than one potential energy surface) in vacuo one must add the complications associated to the presence of a solvent, that is, the great number of surrounding molecules that interact with the solute molecule and the existence of a manifold of configurations thermally accessible that must be included to obtain statistically significant results.

Furthermore, when one studies emission spectra it is necessary to take into account the subtle interplay between the time evolution of the excited state and the dynamics of the solvent, something that does not occur in the study of UV-vis absorption spectra. A photophysical or photochemical process usually begins with the excitation from the minimum energy configuration of the ground state to the Franck–Condon (FC) point on the excited state free energy surface. The classical formulation of this principle establishes that in the time required for a radiative process to occur ($\approx 10^{-15}$ s), the geometry of the molecule, and of the solvent around it, remains fixed. This means that, at the FC point, the solvent is in a non-equilibrium situation whose structure corresponds to the equilibrium with the solute in its ground state. After the absorption process, and as time goes on, the solvent modifies its structure and after a long enough time it becomes equilibrated with the charge distribution of the solute excited state. The time scale of the different processes involved in the evolution of an excited state can be very different. For instance, the lifetimes of most emitting states are sufficiently long (1 ns or larger) to permit a complete

relaxation of the solute and the solvent. Only when the emission involves excited states characterized by very short lifetimes or solvents with high viscosity must we expect an incomplete relaxation of the solvent. Radiationless processes are usually faster, they can take place on the femtosecond time scale, a scale in which, in general, the solvent equilibration will not be complete. However, in systems where the geometry of the surface crossing points is very different from the FC point the de-excitation will take place only after a great part of the solvent reorganization has occurred.

We can hence define two limit cases depending on whether the solvent is in an equilibrium or non-equilibrium situation. In a real system, and depending on the specific characteristics of the process, we can find the solvent structure at any point between these two limits. It is important to stress that, actually, the solvent dynamics is characterized by different response times, associated to different solvent degrees of freedom. Traditionally, it has become usual to distinguish between an inertial component, associated to nuclear movements (vibrations, rotations and translations) and an inertialess or electronic component, associated to the response of the electronic degrees of freedom of the solvent (although more complex classifications are possible) [6,19,20]. In general it is supposed that the electronic response is fast enough so as to be always in equilibrium with the solute charge distribution even in the FC point. In dielectric continuum models [19,21] these two types of response have been usually characterized by the square of the index of refraction in the case of the electronic component or by the dielectric constant at zero frequency in the case of the complete response (inertial plus electronic). In molecular solvent models, the electronic component can be conveniently represented through electronic polarizabilities on the individual solvent molecules.

In the following, we present a sequential quantum mechanics/molecular mechanics (QM/MM) method, known as ASEP/MD [22,23,24,25,26], oriented to the study of solvent effects on absorption and emission spectra and on non-radiative excited state decay. The method combines a high-level quantum-mechanic description of the ground and excited states of the solute molecule with a molecular mechanics description of the solvent and allows the mutual equilibration of the solute charge distribution and the solvent structure around it. Furthermore, it permits the study of electron transitions in equilibrium and non-equilibrium conditions. The rest of the chapter is organized as follows: Section 2 details the main characteristics of the method, paying special attention to the evaluation of the gradients (ground and excited state gradients, gradient difference, derivative coupling) used in the search of minima and surface crossing points. In Section 3, and taking the acrolein molecule in aqueous solution as a model, we show how the ASEP/MD method permits the study of solvent shifts in absorption and emission spectra as well as the characterization of the competitive radiationless de-excitation pathways. Special attention is dedicated to the comparison between the results obtained assuming equilibrium and non-equilibrium solvation.

6.2. METHOD

6.2.1. Fundament of the ASEP/MD Method

ASEP/MD, acronym for average solvent electrostatic potential obtained from molecular dynamics data, is a sequential QM/MM method that makes extensive use of the mean field approximation (MFA) [24]. In solution, any static property A of the system must be calculated by averaging over the configurational space $\{X\}$ defined by all the configurations thermally accessible to the system:

$$\langle A\rangle = \frac{\sum_i \exp(-E_i/kT)\,\langle\Psi_i|\,\hat{a}\,|\Psi_i\rangle}{\sum_i \exp(-E_i/kT)} \tag{6-1}$$

where $\hat{a}$ is the quantum-mechanic operator for the property A and Ψ_i represents the quantum state i. This means that, in principle, hundreds or thousands of quantum calculations are necessary to obtain results that are statistically significant. In the mean field approximation this average is replaced by the value obtained in the presence of an average perturbation or configuration. The main advantage of MFA is that it greatly reduces the number of quantum calculations needed, the cost that has to be paid is the neglect of the correlation between the motion of the solvent nuclei and the response of the solute electron polarizability, i.e., the MFA does not allow the solute to polarize in response to instantaneous changes in the solvent nuclear configurations as consequence of the thermal fluctuations. It has been shown, both theoretically [24] and experimentally [27] that this correlation energy, usually known as Stark component [28,29], does not contribute significantly to the solvent shift. Many of the most frequently used methods for the study of solvent effects make use of the MFA: the different quantum versions of dielectric continuum models (SCRF [30], PCM [2], multipole expansions [3,4], etc.), the methods based on Langevin dipoles [31] or more elaborated methods such as RISM/SCF [32] are representative examples of this.

In the MFA the average value, $\langle A\rangle$, of any quantity is approximated as

$$\langle A\rangle \approx \bar{A} = \int \bar{\Psi}^*\hat{a}\bar{\Psi}\,\mathrm{d}r \tag{6-2}$$

where $\bar{\Psi}$ is the solute wavefunction perturbed by the solvent and calculated by solving the following effective Schrödinger equation:

$$\left(\hat{H}_{\mathrm{QM}} + \left\langle \hat{H}_{\mathrm{int}}^{\mathrm{elect}}\right\rangle\right)\left|\bar{\Psi}\right\rangle = \bar{E}\left|\bar{\Psi}\right\rangle \tag{6-3}$$

$\hat{H}_{QM}$ being the "in vacuo" solute molecular Hamiltonian and where the solute–solvent electrostatic interaction energy reads

$$\left\langle \hat{H}_{\mathrm{int}}^{\mathrm{elect}}\right\rangle = \int \mathrm{d}r\cdot\hat{\rho}\cdot\langle V_S(r;\rho)\rangle_{\{X\}} \tag{6-4}$$

here $\hat{\rho}$ is the solute charge density operator and the term $\langle V_S(r;\rho)\rangle_{\{X\}}$ is the average solvent electrostatic potential (ASEP) or reaction potential generated by the solvent at the r position. The brackets denote an average on the configurational space $\{X\}$. In general, the ASEP depends on ρ, the solute charge density, consequently, Eqs. (6-3) and (6-4) must be solved iteratively. In defining (6-4) only the electrostatic component was considered, although other components of the solute–solvent interaction energies, dispersion or repulsion terms for instance, can also be included.

Different solvation methods can be obtained depending on the way the $\langle V_S(r;\rho)\rangle_{\{X\}}$ term is calculated. So, for instance, in dielectric continuum models $\langle V_S(r;\rho)\rangle_{\{X\}}$ is a function of the solvent dielectric constant and of the geometric parameters that define the molecular cavity where the solute molecule is placed. In ASEP/MD, the information necessary to calculate $\langle V_S(r;\rho)\rangle_{\{X\}}$ is obtained from molecular dynamics calculations. In this way $\langle V_S(r;\rho)\rangle_{\{X\}}$ incorporates information about the microscopic structure of the solvent around the solute, furthermore, specific solute–solvent interactions can be properly accounted for. For computational convenience, the potential $\langle V_S(r;\rho)\rangle_{\{X\}}$ is discretized and represented by a set of point charges $\{q_i\}$ that simulate the electrostatic potential generated by the solvent distribution. The set of charges $\{q_i\}$ is obtained in three steps [26]:

(1) Each selected solute–solvent configuration is translated and rotated in such a way that all of the solvent coordinates are referred to a reference system centred on the centre of mass of the solute with the coordinate axes parallel to the principal axes of inertia of the solute.

(2) Next, one explicitly includes in the ASEP the charges belonging to solvent molecules that, in any of the molecular dynamics (MD) configurations selected, lie inside a sphere of radius a and that includes at least the first solvation shell. The value of every charge is then divided by the number of solvent configurations included in the determination of the ASEP. Next, in order to reduce the number of charges, one adds together all the charges separated from each other by less than a certain distance. This distance is generally taken as 0.5 a.u.

(3) Finally, one includes a second set of charges representing the effect of the solvent molecules lying outside the first solvation shell. These charges are obtained by a least squares fit to the values of the ASEP originated by the outer solvent molecules in a three-dimensional grid defined inside the volume occupied by the solute molecule. The solute volume is defined through a set of interlocking spheres of radius $f{\cdot}R_{\mathrm{vdw}}$, where f is a numerical factor close to one and R_{vdw} are the Bondi radii [33]. The total number of charges introduced into the perturbation Hamiltonian is generally between 25 000 and 35 000.

The basic scheme of ASEP/MD is displayed in Figure 6-1. ASEP/MD alternates high-level quantum calculations and MD simulations in an iterative procedure. During the MD simulations the internal geometry and charge distribution of the solute molecule, as well as those of the solvent molecules, are considered as fixed. From the MD data one obtains the average solvent electrostatic potential, $\langle V_S(r,\rho)\rangle$ that is introduced as a perturbation into the solute molecular Hamiltonian. By solving the associated Schrödinger equation, one gets a new solute charge distribution that

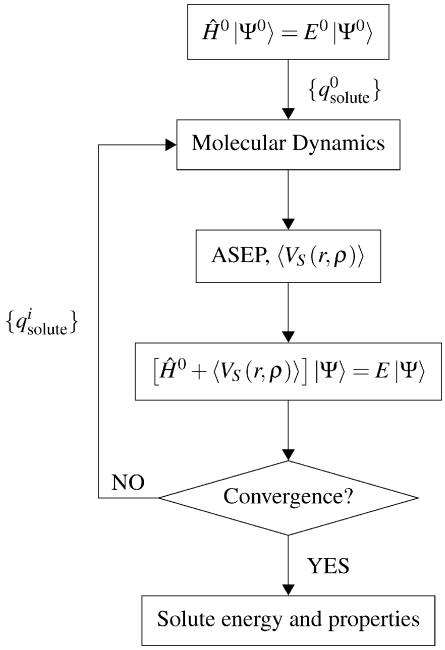

Figure 6-1. Scheme of the ASEP/MD method

serves as input for a new MD calculation. The process is repeated until convergence in the solute charges and in the solute energy is reached. At the end of this process the solute charge distribution and the solvent structure around it become mutually equilibrated. The charges that represent the solute molecule during the MD simulation can be obtained from the in solution molecular wavefunction by using the CHELPG method [34,35] or any of the many methods currently available.

In ASEP/MD, the MD simulations can be performed using polarizable or non-polarizable solvents. However, it is known that simulations employing effective charges can reproduce adequately the solvent structure and are more effective from a computational point of view than those using polarizable force fields. Because of this, in ASEP/MD the solvent polarization is made a posteriori. The determination of the solvent electron polarization with the ASEP/MD method involves two steps [36]. During the first step the solvent structure around the solute is equilibrated, but it is supposed that the charge distribution of every solvent molecule remains fixed, that is, during the simulations one considers a non-polarizable solvent. In the second step, the solvent structure is kept fixed but now the electron degrees of freedom of the solvent polarize in response to the changes in the solute charge distribution originated, for instance, by an electron transition in the solute. That is, using the solvent structure and solute geometry obtained in the first step, in the second one the quantum-mechanical solute and the solvent electron polarization are coupled. To this end, we assign a molecular polarizability to every solvent molecule and,

simultaneously, replace the effective solvent charge distribution used in the MD calculation (TIP3P [37] for instance, if the solvent is water) with the gas phase charge distribution. This is necessary because effective charges include a certain degree of implicit solvent polarization; when one considers a polarizable model it is necessary to use the in vacuo charges of the solvent molecules in order to avoid accounting twice for this effect.

6.2.2. Ground and Excited State Gradients

Any method dedicated to the study of solvent effects on electron spectra must permit the geometry optimization of the solute both in the ground and excited states in presence of the perturbation originated by the solvent. ASEP/MD uses a variant of the free energy gradient method [38,39,40] for the calculation of the gradients that drive the optimization process. The bases of the method are the following: Let $G = -kT \ln Z_{\mathrm{NVT}}$ be the Helmholtz free energy of a system formed by one solute molecule and N–1 solvent molecules. Z_{NVT} is the quasi-classical canonical partition function defined by:

$$Z_{\mathrm{NVT}} = \frac{1}{N!}\frac{1}{h^{3N}} \int \mathrm{d}R^N \mathrm{d}p^N \exp\left[-\frac{E(p^N, r^N)}{kT}\right] \tag{6-5}$$

where E is the energy of the system, which, by convenience, can be split into three terms:

$$E = E_{\mathrm{QM}} + E_{\mathrm{int}} + E_{\mathrm{solv}} \tag{6-6}$$

corresponding to the solute, E_{QM}, the solvent, E_{solv}, and the interaction between them, E_{int}. The force, F, on the free energy surface (the force felt by the solute molecule) is

$$F(R) = -\frac{\partial G}{\partial R} = -\left\langle \frac{\partial E}{\partial R} \right\rangle = -\left\langle \frac{\partial E_{\mathrm{QM}}}{\partial R} \right\rangle - \left\langle \frac{\partial E_{\mathrm{int}}}{\partial R} \right\rangle \tag{6-7}$$

R being the nuclear coordinates of the solute and where we have assumed that E_{solv} does not explicitly depend on the nuclear solute coordinates. The brackets denote a configurational average.

In the same way the Hessian reads

$$\begin{aligned} H(R, R') &= \left\langle \frac{\partial^2 E}{\partial R \partial R'} \right\rangle - \beta \left\langle \frac{\partial E}{\partial R} \right\rangle \left\langle \frac{\partial E}{\partial R} \right\rangle^{\mathrm{T}} + \beta \left\langle \frac{\partial E}{\partial R} \right\rangle \left\langle \frac{\partial E}{\partial R} \right\rangle^{\mathrm{T}} \\ &= \left\langle \frac{\partial^2 E}{\partial R \partial R'} \right\rangle - \beta \left[\langle F^2 \rangle - \langle F \rangle^2 \right] \end{aligned} \tag{6-8}$$

where the superscript T denotes the transposition and β=1/kT. The last term in Eq. (6-8) is related to the thermal fluctuations of the force.

Next, we use the MFA to simplify the gradient and Hessian expressions. Thus, we replace the configurational average of the derivatives with the derivative of the average configuration, furthermore we neglect the force fluctuation terms (given that the Hessian is used only to accelerate the optimization procedure, this approximation has no effect on the optimized geometries but it can affect the harmonic frequencies evaluation). The validity of these approximations has been checked elsewhere [41]. The force and Hessian now read

$$F(R) = -\left\langle \frac{\partial E}{\partial R} \right\rangle \approx -\frac{\partial \bar{E}}{\partial R} = -\frac{\partial \bar{E}_{\mathrm{QM}}}{\partial R} - \frac{\partial \bar{E}_{\mathrm{int}}}{\partial R} \tag{6-9}$$

$$H(R, R') \approx \frac{\partial^2 \bar{E}}{\partial R \partial R'} = \frac{\partial^2 \bar{E}_{\mathrm{QM}}}{\partial R \partial R'} + \frac{\partial^2 \bar{E}_{\mathrm{int}}}{\partial R \partial R'} \tag{6-10}$$

where $\bar{E}$ and its components are calculated as the solution of the Eq. (6-3).

From a computational point of view, it is convenient to split the interaction term into two components, one associated to the electrostatic interaction and the other to the van der Waals contribution:

$$\hat{H}_{\mathrm{int}} = \hat{H}_{\mathrm{int}}^{\mathrm{elect}} + \hat{H}_{\mathrm{int}}^{\mathrm{vdw}} \tag{6-11}$$

The $\hat{H}_{\mathrm{int}}^{\mathrm{elect}}$ term is calculated using Eq. (6-4), while the $\hat{H}_{\mathrm{int}}^{\mathrm{vdw}}$ term is represented by a Lennard-Jones (LJ) potential. This last term depends only on the nuclear coordinates and hence has no effect on the solute wavefunction but it contributes to the final value of the gradient and Hessian. The final expression for the force is

$$F(R) = -\frac{\partial \bar{E}_{\mathrm{QM}}}{\partial R} - \frac{\partial \bar{E}_{\mathrm{int}}^{\mathrm{elect}}}{\partial R} - \left\langle \frac{\partial E_{\mathrm{int}}^{\mathrm{vdw}}}{\partial R} \right\rangle \tag{6-12}$$

with an equivalent expression for the Hessian. As we can see, electrostatic and van der Waals contributions are calculated in a different way. In the case of the electrostatic term the gradient is calculated quantum-mechanically as the gradient of the average solvent configuration, however, the van der Waals contribution is calculated with a classical force field during the MD simulation as the average value of the gradient over all solvent configurations selected.

When one supposes equilibrium solvation, the different terms appearing in Eq. (6-12) are calculated using the configurational space of each state. For instance, for an excited state we have

$$F^{\mathrm{ex}}(R) = -\nabla \bar{E}(R) = -\frac{\partial \bar{E}_{\mathrm{QM}}(\rho^{\mathrm{ex}})}{\partial R} - \frac{\partial \bar{E}_{\mathrm{int}}^{\mathrm{elect}}(\rho^{\mathrm{ex}}, \{X^{\mathrm{ex}}\})}{\partial R} - \left\langle \frac{\partial E_{\mathrm{int}}^{\mathrm{vdw}}}{\partial R} \right\rangle_{\{X^{\mathrm{ex}}\}} \tag{6-13}$$

where we have made explicit the functional dependence of the energy with the solute charge density and where $\{X^{\mathrm{ex}}\}$ indicates that the average solvent structure is calculated using the solvent configurations in equilibrium with the charge distribution of the solute excited state, ρ^{ex}. However, in FC points, characterized by a non-equilibrium solvation situation, the configurational space used is that of the ground state (for an absorption process), and the force can then be written as

$$F^{\mathrm{FC}}(R) = -\nabla \bar{E}(R) = -\frac{\partial \bar{E}_{\mathrm{QM}}(\rho^{\mathrm{ex}})}{\partial R} - \frac{\partial \bar{E}_{\mathrm{int}}^{\mathrm{elect}}(\rho^{\mathrm{ex}}, \{X^{\mathrm{gr}}\})}{\partial R} - \left\langle \frac{\partial E_{\mathrm{int}}^{\mathrm{vdw}}}{\partial R} \right\rangle_{\{X^{\mathrm{gr}}\}} \tag{6-14}$$

where now $\{X^{\mathrm{gr}}\}$ is the solvent configuration in equilibrium with the charge distribution of the solute ground state.

6.2.3. Location of Conical Intersections and Singlet–Triplet Crossing Points in Solution

To locate a minimal energy conical intersection (MECI) between two electronic states K and L we combine the ASEP/MD method with an algorithm due to Bearpark et al. [42]. The algorithm simultaneously minimizes the in solution energy difference between the two intersecting states and the energy of the crossing seam between the two potential energy surfaces. The final form taken by the gradient used in the location algorithm is

$$\mathbf{f}_{KL} = 2(E_K - E_L)\hat{g}_{KL} + \left[\nabla E_K - (\nabla E_K \cdot \hat{g}_{KL})\,\hat{g}_{KL} - \left(\nabla E_K \cdot \hat{h}_{KL}\right)\hat{h}_{KL}\right] \tag{6-15}$$

here E_K and E_L are the energies of the intersecting surfaces, ∇E_K is the gradient of the upper state and $\hat{g}_{KL}$ and $\hat{h}_{KL}$ are the two versors that define the branching space or g–h plane [43], i.e., the subspace of nuclear coordinates in which the degeneracy between the two intersecting surfaces is lifted linearly in displacements from the intersection. When the two intersecting states have different spin symmetry as in the case of singlet–triplet crossing (STC), the $\hat{h}_{KL}$ term vanishes and only one coordinate defines the branching space. The expression of $\mathbf{g}_{KL}$, the energy difference gradient vector, is

$$\mathbf{g}_{KL} = \nabla(E_K - E_L) \tag{6-16}$$

while $\mathbf{h}_{KL}$, the derivative coupling vector, reads

$$\mathbf{h}_{KL} = \langle \Psi_K \,|\nabla|\, \Psi_L \rangle \tag{6-17}$$

where the gradient ∇ is a vector in the nuclear space and Ψ_I are the adiabatic electronic wavefunctions, eigenfunctions of the electronic Hamiltonian, $\hat{H}$, with energies E_I. The corresponding versors are defined as $\hat{g}_{KL} = \mathbf{g}_{KL} / |\mathbf{g}_{KL}|$ and $\hat{h}_{KL} = \mathbf{h}_{KL} / |\mathbf{h}_{KL}| - \left(\mathbf{h}_{KL}\hat{g}_{KL} / |\mathbf{h}_{KL}|\right) \hat{g}_{KL}$.

Equation (6-15) is valid both for in vacuo and in solution systems. Obviously, in this last case we must include the perturbation due to the solvent in each one of the terms: interstate energy difference, excited state gradient, energy difference gradient and derivative coupling.

The energies of the K and L states are obtained by solving Eqs. (6-3) and (6-4), the excited state gradient is calculated with Eq. (6-13). The same expression is used in the calculation of the energy difference gradient, $\mathbf{g}_{KL}$, however, in this case some simplifications are possible because we suppose that the Lennard-Jones coefficients are the same for all the states of one molecule. Furthermore, taking into account that the two states K and L are calculated at the same geometry we obtain

$$\begin{aligned}\mathbf{g}_{KL} = \nabla(E_K - E_L) = \frac{\partial \bar{E}_{\mathrm{QM}}(\rho^K)}{\partial R} - \frac{\partial \bar{E}_{\mathrm{QM}}(\rho^L)}{\partial R} \\ + \frac{\partial \bar{E}^{\mathrm{elect}}_{\mathrm{int}}(\rho^K, \{X^K\})}{\partial R} - \frac{\bar{E}^{\mathrm{elect}}_{\mathrm{int}}(\rho^L, \{X^K\})}{\partial R}\end{aligned} \tag{6-18}$$

where the van der Waals terms vanish because they depend only on nuclear coordinates and hence take the same values for all the electronic states. Note that we use the configurational space of the excited state K in the determination of the solute–solvent interaction energy difference.

The complete scheme of the process followed to locate CI or STC of molecules in solution using ASEP/MD is shown in Figure 6-2. We begin by equilibrating the solvent and the solute and getting a set of point charges that represent the charge distribution of the solute molecule in the initial state, generally the ground state. These charges are then used as input for an MD simulation of the solute and solvent molecules, the remaining parameters for the solute (LJ coefficients) and solvent (charges and LJ coefficients) are obtained from the literature. N representative solvent configurations (N usually taken between 500 and 1000) are selected from the MD simulation. From these configurations the average solvent potential, Eq. (6-4), generated by the solvent in the volume occupied by the solute is calculated. Next, one solves the electronic Schrödinger equation of the solute molecule, Eq. (6-3), in presence of the average perturbation generated by the solvent. The energies and wavefunctions of the crossing points are calculated and the gradient $\mathbf{f}_{KL}$ is obtained. A new solute geometry, closer to the crossing point, can be obtained by using a quasi-Newton method. In this point we have two possibilities depending on whether the solvent is in an equilibrium or non-equilibrium situation. In the former case the solvent must be equilibrated with the solute charge distribution of the upper state and hence a new MD must be performed, the procedure is continued until the solvent distribution and the charge distribution of the upper state are mutually equilibrated. Although strictly speaking it is necessary to perform an MD calculation for each new

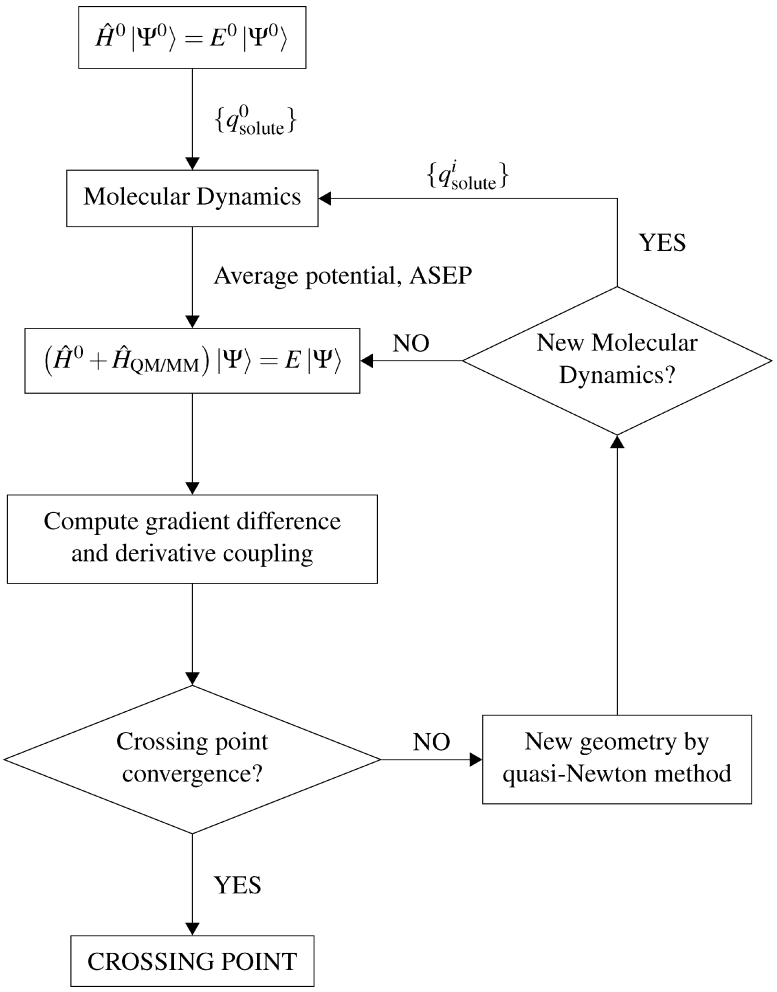

Figure 6-2. Conical intersection and singlet–triplet crossing location scheme

solute geometry, this is a very inefficient procedure. It has been verified [44] that it is computationally more efficient to perform several steps of the crossing point search procedure before equilibrating the solvent again. We update the solvent structure only after 10–20 iterations of the crossing point search procedure.

In the case of non-equilibrium conditions, the crossing point is located for a frozen solvent structure. During an electron transition the Franck–Condon principle is applicable and the solvent nuclei remain fixed during the transition. Consequently, the solvent structure is in equilibrium with the charge distribution of the solute in its ground state. The crossing point search procedure is performed in presence of this solvent structure.

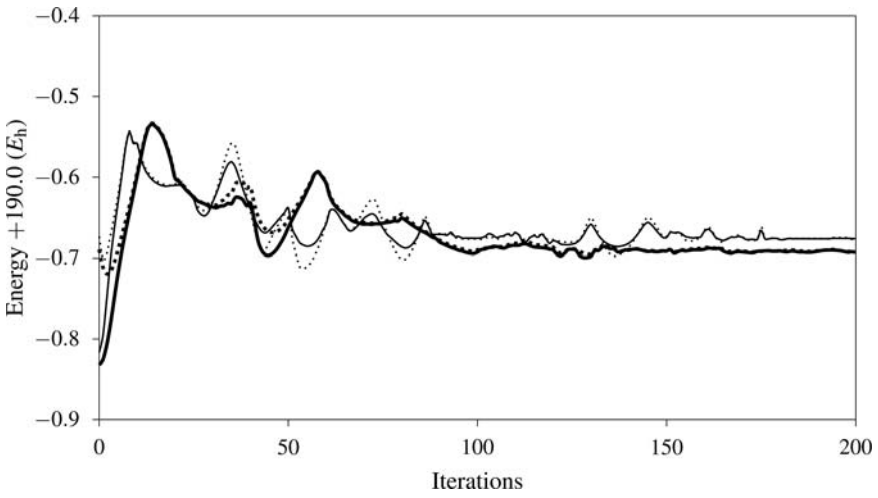

Figure 6-3. Evolution during the search procedure of the S_0 and S_1 energies of acrolein (in Hartree) in vacuum (*thin lines*, *continuous* and *dotted*, respectively), and in water solution (*thick lines*, *continuous* and *dotted*, respectively)

Figure 6-3 displays the evolution of the total energy in vacuo and in solution of the S_0 and S_1 acrolein states as a function of the number of cycles of the search procedure. In the first steps the energy difference between the two crossing states decreases until the system is close to the CI seam. Then the energy decreases until the MECI is reached. Each time a new ASEP/MD is performed the solvent structure is recalculated. If this change is important the position of the crossing seam changes and the energies begin to fluctuate until they are again stabilized in a new plateau. The final in solution values (energies, geometries, dipoles, etc.) are calculated by averaging over the results obtained with the last few cycles of ASEP/MD.

6.2.4. Free Energy Differences

Once the different minima, MECI and MESTC points have been located, it is necessary to determine their relative stabilities. For in solution systems the relevant quantity is the free energy difference. The standard free energy difference between two states, *i* and *f*, in solution can be written as the sum of two terms [45]

$$\Delta G_{\text{diff}} = \Delta G_{\text{solute}} + \Delta G_{\text{int}} \tag{6-19}$$

where ΔG_{int} is the difference in the solute–solvent interaction free energy between the two QM states, and

$$\Delta G_{\text{solute}} = \Delta E_{\text{solute}} + \Delta V_{\text{solute}} \tag{6-20}$$

where

$$\Delta E_{\text{solute}} = E^{f}_{\text{QM}} - E^{i}_{\text{QM}} = \left\langle \bar{\Psi}^{f} \middle| \hat{H}_{\text{QM}} \middle| \bar{\Psi}^{f} \right\rangle - \left\langle \bar{\Psi}^{i} \middle| \hat{H}_{\text{QM}} \middle| \bar{\Psi}^{i} \right\rangle \tag{6-21}$$

is the ab initio difference between the two QM states calculated using the in vacuo solute molecular Hamiltonian, $\hat{H}_{\text{QM}}$, and the in solution wavefunctions. ΔV_{solute} is the solute's vibrational and thermal contribution to the free energy (usually evaluated with the harmonic approximation).

In order to clarify the role played by the solvent in the stabilization of the different structures it is useful to split the ΔG_{int} term into two terms: ΔE_{int} and ΔG_{solv}. The last term, ΔG_{solv}, provides the solvent distortion energy, i.e., the energy spent in changing the solvent structure from the initial to the final state. The term ΔE_{int} accounts for the difference in the solute–solvent interaction energy between the final and initial states. For a non-polarizable solvent this term reads

$$\Delta E_{\text{int}} = E^{f}_{\text{int}} - E^{i}_{\text{int}} = \left\langle \bar{\Psi}^{f} \middle| \hat{H}_{\text{int}} \middle| \bar{\Psi}^{f} \right\rangle - \left\langle \bar{\Psi}^{i} \middle| \hat{H}_{\text{int}} \middle| \bar{\Psi}^{i} \right\rangle \tag{6-22}$$

If one wants to consider explicitly the electron polarization of the solvent it is necessary to add to Eq. (6-22) the energy spent in polarizing the solvent dipoles. In a previous work [36], we have shown that for a polarizable solvent, the final expression that the solute–solvent interaction energy takes is

$$\Delta E^{\text{pol}}_{\text{int}} = \frac{1}{2}\Delta E_{q\mu} + \Delta E_{\rho q} + \frac{1}{2}\Delta E_{\rho\mu} \tag{6-23}$$

Here, q refers to the permanent charges of solvent molecules, μ the induced dipoles on the solvent and ρ the solute charge density.

In solvent effect studies, a fundamental quantity is the solvent shift, δ, on the energy, defined as the difference between the energy gap values calculated in solution and in vacuo:

$$\delta = \Delta G_{\text{diff}} - \Delta G^{0}_{\text{solute}} \tag{6-24}$$

If we suppose, as it is usually the case, that the solvent has only a small influence on the solute's thermal contribution, ΔV_{solute}, then, using Eqs. (6-19) and (6-20), Eq. (6-24) can be simplified to

$$\delta = \Delta G_{\text{int}} + (\Delta E_{\text{solute}} - \Delta E^{0}_{\text{solute}}) \tag{6-25}$$

where the term in parentheses is the distortion energy of the solute: the energy spent in the solute polarization during the solvation process. Splitting the different contributions to ΔG_{int} one obtain the following expression for the solvent shift on a solute embedded in a polarizable solvent:

$$\delta = \frac{1}{2}\Delta E_{\mu q} + \Delta E_{\rho q} + \frac{1}{2}\Delta E_{\rho\mu} + (\Delta E_{\text{solute}} - \Delta E^{0}_{\text{solute}}) + \Delta G_{\text{solv}} \tag{6-26}$$

In the case of vertical transitions the term ΔG_{solv} cancels out because the Franck–Condon approximation is applicable and the solvent structure is the same in both the ground and excited states. For non-vertical transition, ΔG_{solv} must be explicitly calculated. We calculate this term as difference between ΔG_{int} and ΔE_{int}. This last term is calculated quantum-mechanically using Eq. (6-22). The ΔG_{int} can be calculated using free energy perturbation method [46]. The solute geometry is assumed to be rigid and a function of the perturbation parameter (λ) while the solvent is allowed to move freely. When λ=0 the solute geometry and charges and the solute–solvent interaction parameters correspond to the initial state. When λ=1 the charges and geometry are those of the final state. For intermediate values a linear interpolation is applied.

6.3. DE-EXCITATION PATHWAYS IN ACROLEIN

As an example of application of the ASEP/MD method described in the previous section, in this section we proceed to the discussion of solvent effects on radiative and non-radiative processes in acrolein. Acrolein or propenal is the smallest α,β-unsaturated carbonyl compound. The presence of the carbonyl group and the C=C double bond makes it a compound of marked interest from a spectroscopic and photochemical points of view. In solution, acrolein displays a strong absorption band corresponding to a $^1(\pi\rightarrow\pi^*)$ transition and a weak band, at lower frequencies associated to a dipole forbidden $^1(n\rightarrow\pi^*)$ transition. The fluorescence spectrum shows a band, which overlaps the first absorption peak, and which is assigned as originating from the S_1 state. The molecule presents also a phosphorescence spectrum, but the assignation of the observed band to one specific transition is not clear. Finally, the small values of the quantum yields for both fluorescence and phosphorescence (0.007 and 0.00004, respectively [47]) point to the existence of important non-radiative decay pathways.

In what follows, the ground and excited states of acrolein have been described using CASSCF and CASPT2 levels of theory. In previous papers [36,48] it was shown that the inclusion of the dynamic correlation component through CASPT2 calculations is compulsory if one desires to reproduce the transition energy. However, in the acrolein case this component does not appreciably modify the solvent shift and, in general, a good description of the solvent effects can be obtained at CASSCF level. The complete active space was spanned by all the configurations arising from six valence electrons in five orbitals (6e/5o). The quantum calculations were performed using two basis sets: the 6-31 G* basis set and an atomic natural orbitals (ANO) [49] basis set (the contraction scheme used was C,O [4s3p1d]/H [2s1p]). The initial geometry for acrolein was obtained by CASSCF optimization both in vacuum and in solution with the aforementioned basis sets. A total of one acrolein molecule and 250 TIP3P water molecules [37] were simulated with fixed intramolecular geometry by combining LJ interatomic interactions with electrostatic interactions in a cubic box of 18.7 Å side. Periodic boundary conditions were applied, and spherical cutoffs were used to truncate the molecular interactions at 9.0 Å. A time step of 0.5 fs

was used. The electrostatic interaction was calculated with the Ewald method. The temperature was fixed at 298 K by using a Nosé-Hoover thermostat. Each MD calculation simulation was run for 75 ps (25 ps equilibration, 50 ps production). Solvent effects were treated with the ASEP/MD program [26,41] using the data provided by Gaussian 98 [50] (quantum calculations) and MOLDY [51] (MD simulations). CASPT2 calculations were performed with the Molcas [52] program.

6.3.1. Absorption Spectra

To understand the nature of the solvent shift in the absorption process it is interesting to analyse first the solvent structure around the acrolein molecule. The radial distribution functions (rdf) O(water)–O(acrolein) and H(water)–O(acrolein) for S_0 and S_1 states are shown in Figures 6-4 and 6-5, respectively. They were obtained as average values over the last 10 ASEP/MD cycles. For the S_0 state, the H(w)–O(a) rdf displays a well-defined peak at 1.85 Å, indicating a strong hydrogen bond between acrolein and a water molecule. The first peak of the O(w)–O(a) rdf appears at 2.75 Å, and given that the H–O distance in water is 0.957 Å, one can conclude that the hydrogen bond is almost linear. In Figure 6-4, it can also be observed that the radial distribution function has several peaks at long distances, indicating that acrolein imposes a considerable order on the water structure. The calculated coordination number is 2.1. The two electron lone pairs of the acrolein oxygen seem to be involved in the formation of hydrogen bonds.

Table 6-1 lists the solvent shift on the $^1(n\rightarrow\pi^*)$ transition and its different contributions (see Eq. (6-26)). The first column corresponds to the solvent shift due to

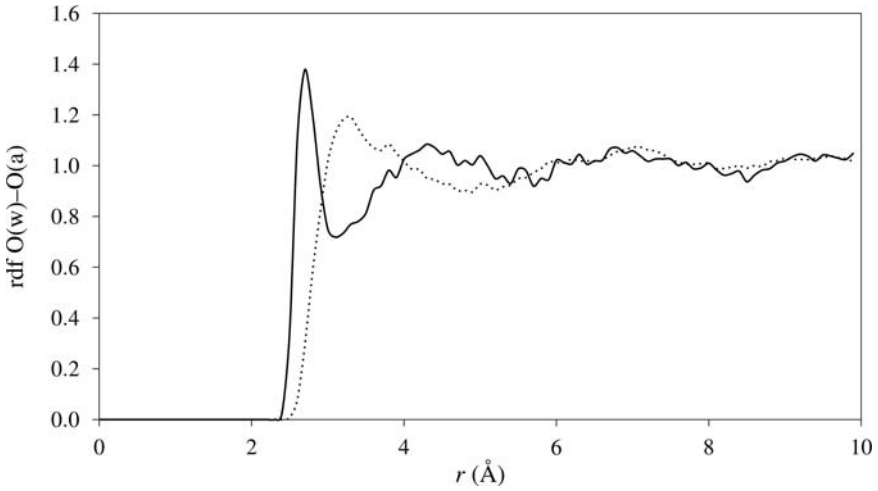

Figure 6-4. Oxygen (water)–oxygen (acrolein) radial pair distribution function of the S_0 (*continuous line*) and S_1 (*dotted line*) states of acrolein

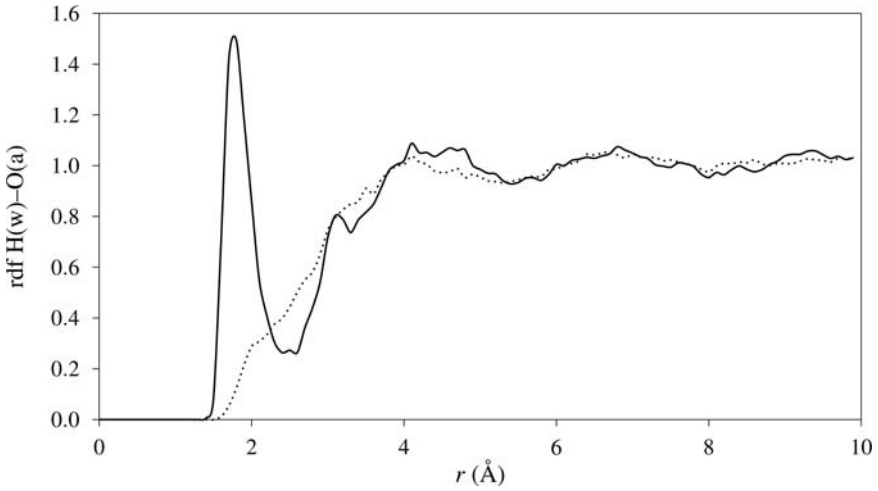

Figure 6-5. Hydrogen (water)–oxygen (acrolein) radial pair distribution function of the S_0 (*continuous line*) and S_1 (*dotted line*) states of acrolein

the electrostatic interaction between the solute charge distribution and the permanent charges of the solvent. The second and third columns correspond to the interaction between the induced solvent dipoles (μ) and the solute charge distribution (ρ) and permanent solvent charges (q). The fourth column is the contribution of the solute distortion energy. The total solvent shift is given in the last two columns. Given that the dipole moment, and hence the solute–solvent interaction energy, decreases in about 2.2 D during the excitation, the band position is blue shifted in 5.0 kcal/mol (6-31 G* basis set), very close to the value, 4.5 kcal/mol, obtained at CASPT2 level and using ANO basis sets and to the experimental value [53], 4.4 kcal/mol. The largest contribution to the solvent shift comes from the interaction between the solute and the permanent charges of the solvent. However, the contribution from the solvent polarization (components associated to the induced dipoles) is also important, representing about 26% of the total solvent shift.

In solution, the strongest band of the absorption spectrum is associated with the $^1(\pi\rightarrow\pi^*)$ transition. During this transition the dipole moment increases in about 2.0 D, and the position of the band is red shifted by 6.2 kcal/mol.

Table 6-1. Solvent shift values and its components in kcal/mol

	$\delta_{\rho q}$	$\frac{1}{2}\delta_{q\mu}$	$\frac{1}{2}\delta_{\rho\mu}$	δ_{sol}^{dist}	δ	δ_{CASPT2}
Absorption	5.9±0.4	0.04±0.02	1.1±0.1	–2.7±0.4	4.3±0.2	4.5±0.2

6.3.2. Emission Spectra

As was indicated above the fluorescence band overlaps the $^1(n\rightarrow\pi^*)$ absorption band, this fact and the very low value of the fluorescence quantum yield allows the assignation of the band to the de-excitation from the S_1 state. The charge flux that accompanies the electron transition has an influence on the solvent structure around the excited state of the acrolein molecule. Figures 6-4 and 6-5 display the O(water)–O(acrolein) and H(water)–O(acrolein) radial pair distribution function in the S_1 excited state with dotted lines. In the O(w)–O(a) rdf the height of the first peak decreases with the excitation and its position is shifted to longer distances, the same is valid for the rest of the peaks, the solvent is less structured around the excited state than around the ground state. The number of solvent molecules included in the first solvation shell (calculated by integration until the first minimum of the ground state rdf) are 2.1 and 1.2 for the ground and excited states, respectively. The behaviour of the H(w)–O(a) rdf is even more striking, the solvent structure found around the solute ground state is completely lost in the solute excited state. One can conclude that the $^1(n\rightarrow\pi^*)$ excitation produces the partial desolvation of acrolein. This desolvation determines the energetic features of the emission process in solution.

Compared to the corresponding in vacuo transition, the solvent originates a blue shift in the fluorescence band of 1.8 kcal/mol (polarizable solvent). The results obtained with polarizable solvent are similar to that obtained with an effective charges model, the computational cost being notably lower in the latter case. The difference in solvent shift values found for the absorption and emission processes is related to the different strengths of the solute–solvent interaction in the ground and first excited states. As it was indicated above, the charge flux that accompanies the excitation yields a lower dipole moment, weaker solvent structure around the solute and as a consequence lower solute–solvent interaction energy (and energy differences) when the solvent is in equilibrium with the excited state. The inclusion of dynamic electron correlation increases the solvent shift by only 0.2 kcal/mol for the absorption process but by 0.6 kcal/mol for the emission process. On a percentage basis, the contribution of the dynamic electron correlation to the solvent shift represents 33% of the total solvent shift in the emission process but less than 5% of the total solvent shift in the absorption process.

The phosphorescence band is more complicated to assign. Table 6-2 displays the energy of the singlet and triplet states both in vacuo and in solution. In both cases, the most stable triplet is the $T_{\pi\pi^*}$ state. This state has in its minimum a geometry twisted 90° around the C=C bond. At this geometry the $T_{\pi\pi^*}$ state crosses the ground state and hence it relaxes non-radiatively through an intersystem crossing. Consequently, the phosphorescence emission must be associated to the de-excitation from the $T_{n\pi^*}$ state. Experimentally, the maximum of the phosphorescence band appears at 2.46 eV, our calculations places the emission from the $T_{n\pi^*}$ state at 2.24 eV. The solvent originates a blue shift of about 0.73 kcal/mol. The solvent structure around the $T_{n\pi^*}$ is similar to that of S_1. Like for the S_1 state, the $T_{n\pi^*}$ state is characterized by a charge flux from the oxygen to the carbon skeleton, this charge flux decreases the dipole moment of the excited triplet state with respect to the ground state value. At the

Table 6-2. Energy results in a.u. ΔE and ΔG in kcal/mol

		Vacuum		Solution		
		E	ΔE	ΔG eq	ΔE non-eq	Geometry
S_1	FC	–190.6788	0.0	0.0	0.0	
S_0	Min	–190.8235	–90.8	–95.8		Planar
S_1	Min	–190.7081	–18.4	–20.7		Planar
$T_{n\pi^*}$	Min	–190.7131	–21.5	–22.3		Planar
$T_{\pi\pi^*}$	Min	–190.7278	–35.7	–36.4		Twisted
$S_1/T_{\pi\pi^*}$	STC	–190.7044	–16.1	–19.2	–17.7	Planar
$T_{n\pi^*}/T_{\pi\pi^*}$	CI	–190.7055	–16.7	–19.1	–18.4	Planar
$T_{\pi\pi^*}/S_0$	STC	–190.7275	–30.5	–33.7	–34.2	Twisted
S_1/S_0	CI	–190.6762	+1.6	–1.4	+6.4	Twisted

same time it produces a partial desolvation of the excited state. These two effects destabilize the excited state with respect to the ground state and explain the blue shift.

6.3.3. Non-radiative Excited State Decay

In the radiationless relaxation of acrolein there are at least four states involved [54], the ground state, S_0, the first singlet excited state, S_1, and two triplet states, $T_{\pi\pi^*}$ and $T_{n\pi^*}$. Two paths have been proposed in order to explain the radiationless de-excitation of acrolein in gas phase: (1) a direct de-excitation through a S_1/S_0 IC and (2) an indirect path starting with a $S_1/T_{\pi\pi^*}$ ISC. From here we have several possibilities: (a) the system can return to the ground state through a $T_{\pi\pi^*}/S_0$ ISC, (b) the system can pass to $T_{n\pi^*}$ through a $T_{\pi\pi^*}/T_{n\pi^*}$ IC. From $T_{n\pi^*}$ acrolein relaxes non-radiatively to $T_{\pi\pi^*}$ and from here it returns to S_0 through a $T_{\pi\pi^*}/S_0$ ISC. When the system is in $T_{n\pi^*}$ state it can relax radiatively originating the phosphorescence band.

Table 6-2 provides the relative stability of the different minima, MECI and MESTC points, calculated in vacuo and in solution, and in the latter case, in equilibrium and non-equilibrium conditions. Figure 6-6 displays the geometries of the minima, and minimal energy CI and STC points.

We first analyse the influence of the solvent on the different geometries supposing solvent equilibrium conditions. In all the cases analysed – minima, MECI and MESTC – the solvent increases the C–O distance and decreases the two C–C distances. This behaviour can be explained by the formation of hydrogen bonds between the carbonyl oxygen and the hydrogen of the water molecules. The larger distance variations appear in the $S_0/T_{\pi\pi^*}$ STC and $T_{\pi\pi^*}/T_{n\pi^*}$ CI. In order to understand the variation of the geometrical parameters it is necessary to consider two variables: the bond order of the carbonyl group and the in vacuo dipole moment value. The

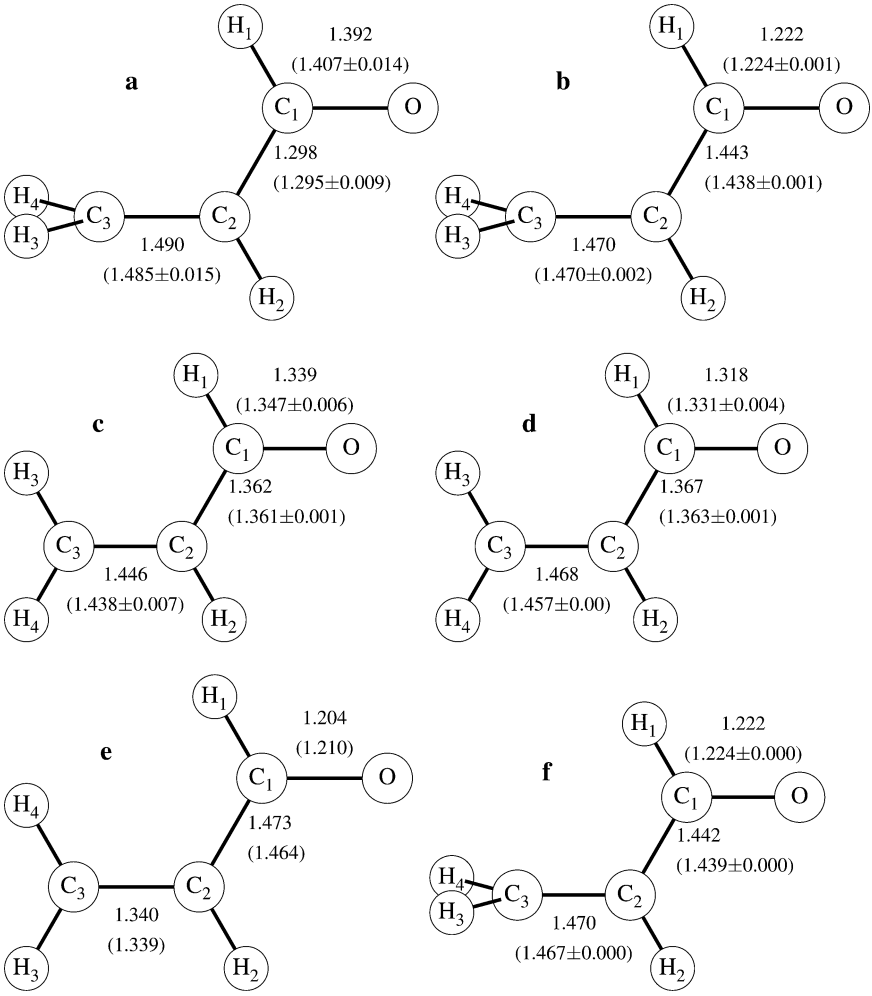

Figure 6-6. (a) S_1/S_0 CI geometry in vacuo and in solution (in parentheses). (b) The $T_{\pi\pi^*}/S_0$ STC geometry in vacuo and in solution (in parentheses). (c) $S_1/T_{\pi\pi^*}$ STC geometry in vacuo and in solution (in parentheses). (d) $T_{n\pi^*}/T_{\pi\pi^*}$ CI geometry in vacuo and in solution (in parentheses). (e) FC geometry in vacuo and in solution (in parentheses). (f) $T_{\pi\pi^*}$ minimum geometry in vacuo and in solution (in parentheses) Distances in Å

larger variations of distances appear in those structures where the C–O bond has a single bond character and the dipole moment is high. In these conditions the bond is more labile and hence easier to elongate. In twisted structures, the solvent affects the $C_1C_2C_3H_6$ torsion angle value, which, in the S_0/S_1 CI structure, for instance, increases from 100° to 103°.

The solvent has also effects on the relative energies of the minima and crossing points. In Table 6-2, all data have been referred to the FC points (in vacuo and in solution), being the points where the de-excitation process initiates. As a general rule and when compared with the in vacuo values, the solvent stabilizes the energy of all the minima and crossing points of acrolein. In the FC point the solvent is in a non-equilibrium situation, however, in the rest of points, minima, CI and STC, the solvent is in equilibrium with the corresponding solute charge distribution. The relaxation of the solvent from a non-equilibrium situation to an equilibrium situation explains the additional stability obtained in solution.

The main conclusion that one can obtain from Table 6-2 is that, in solution, the radiationless relaxation can follow the same path as in vacuo. The direct de-excitation, path 1, through the S_0/S_1 CI is improbable but possible, it is 1.6 kcal/mol above the gas phase FC point but 1.3 kcal/mol below the FC point in solution. However, this path involves an appreciable reorganization of the solvent structure. As for the gas phase process the most probable path passes through the $S_1/T_{\pi\pi^*}$ STC. This de-excitation path supposing an equilibrium solvent situation implies also a large reorganization of the solvent structure around acrolein and hence one can expect that it will be slower in solution than in vacuo.

The different crossing points have also been located for a non-equilibrium solvation situation. Depending on the case, the search procedure can be more complicated than in the equilibrium solvation situation, see Figure 6-7. In non-equilibrium solvation all the crossing points are less stable than the corresponding equilibrium points. For instance, the S_0/S_1 CI is 3.2 kcal/mol above the FC point. However,

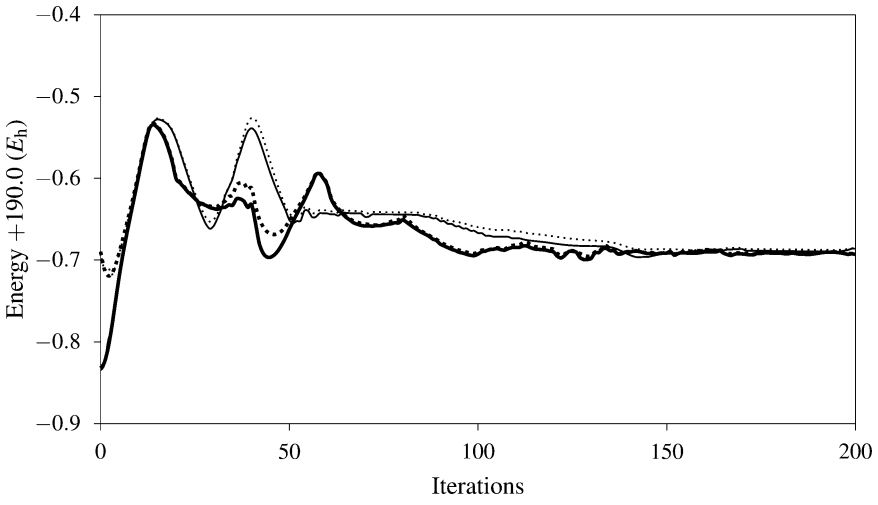

Figure 6-7. Evolution during the search procedure of the S_0 and S_1 energies (in Hartree) in non-equilibrium conditions (*thin lines*, *continuous* and *dotted*, respectively), and in equilibrium conditions (*thick lines*, *continuous* and *dotted*, respectively)

the path that involves the $S_1/T_{\pi\pi^*}$ and $T_{\pi\pi^*}/S_0$ STC is still energetically possible. This path does not imply solvent reorganization, only solute movements and hence can take place, in principle, at practically the same speed as in vacuo. In conclusion, the radiationless relaxation of acrolein in aqueous solution can follow the same path as that of the in vacuo system and must proceed with almost the same speed.

6.4. CONCLUDING REMARKS

In the last decades, the theoretical study of solvent effects has known a great development. New and improved models have been proposed that have permitted to extend the range of problems treated and improve the accuracy of the predictions made. The new models are characterized by a quantum-mechanics high-level description of the solute molecule and a detailed description of the microscopic structure of the solvent. Among this trend is placed the method proposed by our group, the ASEP/MD method: a sequential QM/MM method that has as a distinct feature the use of the mean field approximation. ASEP/MD has been successfully applied to the study of solvent effects on chemical reactions, conformational equilibrium and absorption spectra. In this chapter, we have presented an extended version that permits a first approximation to the study of solvent effects on the radiative and non-radiative decay of excited states. These are intrinsically dynamic processes where it is necessary to take into account the interplay between electronic structure and nuclear dynamics. We have undertaken this problem by establishing two limit situations, which we have characterized as equilibrium and non-equilibrium solvation regimes. In the former, we suppose decay times long enough to allow a complete relaxation of the solute and the solvent structures. In the latter, we suppose the decay process is fast enough to prevent the solvent equilibration (although we assume a complete relaxation of the solute). In some situations the solvent behaviour will be halfway between these two limits and an adequate treatment would require the use of more advanced techniques such as ab initio molecular dynamics. We believe, however, that in many cases, the two limits indicated above would be a good approximation to the real situation and valid and interesting information about the solvent effects on the decay processes could be obtained.

As an example of application of the method we have considered the case of the acrolein molecule in aqueous solution. We have shown how ASEP/MD permits a unified treatment of the absorption, fluorescence, phosphorescence, internal conversion and intersystem crossing processes. Although, in principle, electrostatic, polarization, dispersion and exchange components of the solute–solvent interaction energy are taken into account, only the firsts two terms are included into the molecular Hamiltonian and, hence, affect the solute wavefunction. Dispersion and exchange components are represented through a Lennard-Jones potential that depends only on the nuclear coordinates. The inclusion of the effect of these components on the solute wavefunction is important in order to understand the solvent effect on the red shift of the bands of absorption spectra of non-polar molecules or the disappearance of

the Rydberg bands of chromophores in solution. Furthermore, it is supposed that the LJ parameters are the same for all the electron states. Consequently, in our model, LJ components do not contribute to the transition energies. These approximations constitute a limitation of the method that we will try to overcome in the near future.

REFERENCES

1. Bayliss NS, McRae EG (1954) J Phys Chem 58:1002
2. Tomasi J, Persico M (1994) Chem Rev 94:2027
3. Rivail JL, Rinaldi D (1995) In: Leszczynski J (ed) Computational chemistry: review of current trends, World Scientific Publishing, Singapore
4. Cramer CJ, Truhlar DG (1995) In: Lipkowitz KB, Boyd DB (eds) Reviews in computational chemistry, vol VI. VCH Publishers, New York, p 1
5. Martín ME, Sánchez ML, Olivares del Valle FJ, Aguilar MA (2000) J Chem Phys 113:6308
6. Caricato M, Mennucci B, Tomasi J, Ingrosso F, Cammi R, Corni S, Scalmani G (2006) J Chem Phys 124:124520
7. Improta R, Barone V, Santoro F (2007) Angew Chem Int Ed 46:405
8. Lippert E (1957) Z Elektrochem Ber Bunsenges Phys Chem 61:962
9. Lippert E (1961) Angew Chem 73:695
10. Whery EL (1990) In: Guilbault GG (ed) Practical fluorescence, 2 nd edn. Marcel Dekker, Inc., New York, p 127
11. Toniolo A, Ben-Nun M, Martínez TJ (2002) J Phys Chem A 106:4679
12. Toniolo A, Granucci G, Martínez TJ (2003) J Phys Chem A 107:3822
13. Burghardt I, Cederbaum L, Hynes JT (2004) Faraday Discuss 127:395
14. Spezia R, Burghardt I, Hynes JT (2006) Mol Phys 104:903
15. Garavelli M, Rugen F, Ogliano F, Bearpark MJ, Bernardi F, Olivucci M, Robb MA (2003) J Comput Chem 24:1357
16. Frutos LM, Andruniów T, Santoro F, Ferré N, Olivucci M (2007) Proc Natl Acad Sci USA 104:7764
17. Yamazaki S, Kato S (2005) J Chem Phys 123:114510
18. Yamazaki S, Kato S (2006) J Am Chem Soc 129:2901
19. Tomasi J, Mennucci B, Cammi R (2005) Chem Rev 105:2999
20. Caricato M, Ingrosso F, Mennucci B, Tomasi J (2005) J Chem Phys 122:154501
21. Aguilar MA (2001) J Phys Chem A 105:10393
22. Sánchez ML, Aguilar MA, Olivares del Valle FJ (1997) J Comput Chem 18:313
23. Sánchez ML, Martín ME, Aguilar MA, Olivares del Valle FJ (2000) J Comput Chem 21:705
24. Sánchez ML, Martín ME, Fdez. Galván I, Olivares del Valle FJ, Aguilar MA (2002) J Phys Chem B 106:4813
25. Martín ME, Sánchez ML, Olivares del Valle FJ, Aguilar MA (2002) J Chem Phys 116:1613
26. Fdez. Galván I, Sánchez ML, Martín ME, Olivares del Valle FJ, Aguilar MA (2003) Comput Phys Commun 155:244
27. Ghoneim N, Suppan P (1995) Spectrochim Acta 51A:1043
28. Linder B (1967) Adv Chem Phys 12:225
29. Karlström G, Halle B (1993) J Chem Phys 99:8056
30. Tapia O, Goscinski O (1975) Mol Phys 29:1653
31. Warshel A (1991) Computer modelling of chemical reactions in enzymes and solutions, Wiley Interscience Publication, New York
32. Ten-no S, Hirata F, Kato S (1993) Chem Phys Lett 214:391

33. Bondi A (1964) J Phys Chem 68:441
34. Chirlian LE, Francl MM (1987) J Comput Chem 8:894
35. Breneman CM, Wiberg KB (1990) J Comput Chem 11:361
36. Martín ME, Muñoz Losa A, Fdez. Galván I, Aguilar MA (2004) J Chem Phys 121:3710
37. Jorgensen WL, Chandrasekhar J, Madura JD, Impey RW, Klein ML (1983) J Chem Phys 79:926
38. Okuyama-Yoshida N, Nagaoka M, Yamabe T (1998) Int J Quantum Chem 70:95
39. Okuyama-Yoshida N, Nagaoka M, Yamabe T (2000) J Chem Phys 113:3519
40. Hirao H, Nagae Y, Nagaoka M (2001) Chem Phys Lett 348:350
41. Fdez. Galván I, Sánchez ML, Martín ME, Olivares del Valle FJ, Aguilar MA (2003) J Chem Phys 118:255
42. Bearpark MJ, Robb MA, Schlegel HB (1994) Chem Phys Lett 223:269
43. Yarkony DR (2004) In: Domcke W, Yarkony DR, Köppel H (eds) Conical intersections, Advanced Series in Physical Chemistry no. 15, World Scientific, Singapore, p 42
44. Muñoz Losa A, Martín ME, Fdez. Galván I, Aguilar MA (2007) Chem Phys Lett 443:76
45. Fdez. Galván I, Martín ME, Aguilar MA (2004) J Comput Chem 25:1227
46. Kollman PA (1993) Chem Rev 93:2395
47. Becker RS, Inuzuka K, King J (1970) J Chem Phys 52:5164
48. Muñoz Losa A, Fdez. Galván I, Martín ME, Aguilar MA (2006) J Phys Chem B 110:18064
49. Widmark P-O, Malmqvist P-Å, Roos BO (1990) Theor Chim Acta 77:291
50. Frisch MJ, Trucks GW, Schlegel HB, Scuseria GE, Robb MA, Cheeseman JR, Zakrzewski VG, Montgomery Jr. JA, Stratmann RE, Burant JC, Dapprich S, Millam JM, Daniels AD, Kudin KN, Strain MC, Farkas O, Tomasi J, Barone V, Cossi M, Cammi R, Mennucci B, Pomelli C, Adamo C, Clifford S, Ochterski J, Petersson GA, Ayala PY, Cui Q, Morokuma K, Malick DK, Rabuck AD, Raghavachari K, Foresman JB, Cioslowski J, Ortiz JV, Baboul AG, Stefanov BB, Liu G, Liashenko A, Piskorz P, Komaromi I, Gomperts R, Martin RL, Fox DJ, Keith T, Al-Laham MA, Peng CY, Nanayakkara A, Gonzalez C, Challacombe M, Gill PMW, Johnson B, Chen W, Wong MW, Andres JL, Gonzalez C, Head-Gordon M, Replogle ES, Pople JA (1998) Gaussian 98, Rev. A11.3, Gaussian, Inc., Pittsburgh, PA
51. Refson K (2000) Comput Phys Commun 126:310
52. Andersson K, Barysz M, Bernhardsson A, Blomberg MRA, Carissan Y, Cooper DL, Fülscher MP, Gagliardi L, de Graaf C, Hess BA, Hagberg D, Karlström G, Lindh R, Malmqvist P-Å, Nakajima T, Neogrády P, Olsen J, Raab J, Roos BO, Ryde U, Schimmelpfennig B, Schütz M, Seijo L, Serrano-Andrés L, Siegbahn PEM, Stålring J, Thorsteinsson T, Veryazov V, Widmark P-O (2006) Molcas Version 6, University of Lund, Lund, Sweden
53. Moskvin AE (1966) Theor Exp Chem 2:175
54. Reguero M, Olivucci M, Bernardi F, Robb MA (1994) J Am Chem Soc 116:2103